

DETAILED EVIDENCE FOR FLARE-TO-FLARE VARIATIONS OF THE CORONAL CALCIUM ABUNDANCE

J. SYLWESTER

Space Research Centre, Polish Academy of Sciences, ul. Kopernika 11, 51-622, Wrocław, Poland; js@cbk.pan.wroc.pl

J. R. LEMEN

Lockheed Martin Solar and Astrophysics Laboratory, H1-12 B/252, 3251 Hanover Street, Palo Alto, CA 94304; lemen@sag.space.lockheed.com

AND

R. D. BENTLEY, A. FLUDRA,¹ AND M.-C. ZOLCINSKI

Mullard Space Science Laboratory, Holmbury Saint Mary, Dorking, Surrey, RH5 6NT, United Kingdom

Received 1997 September 2; accepted 1998 February 9

ABSTRACT

The analysis of X-ray solar flare spectra obtained by the Bent Crystal Spectrometer on board the *Solar Maximum Mission* satellite is presented. The ratio of the Ca XIX resonance line intensity to the nearby continuum is used to measure the calcium abundance relative to hydrogen (A_{Ca}). A description of the spectroscopic method of determining the absolute calcium abundance is given. Possible instrumental and solar effects that might influence the abundance estimates are evaluated. Over 5000 spectra from more than 100 flares are analyzed. We find a flare-to-flare variation for A_{Ca} that is not correlated with flare size, H α importance, or with several other flare characteristics. For flares observed from two active regions, the observed value of A_{Ca} increases as a function of time. The average for all flares is $\langle A_{\text{Ca}} \rangle = (5.77 \pm 1.41) \times 10^{-6}$. A discussion of investigated correlations of derived A_{Ca} values with several flare characteristics is presented.

Subject headings: Sun: abundances — Sun: corona — Sun: flares — Sun: X-rays, gamma-rays

1. INTRODUCTION

The determination of absolute elemental abundances is one of the fundamental problems of astrophysics. The composition of the solar plasma is one of the primary sources of information for the cosmic elemental abundances. Several spectroscopic methods, covering a wide range of the electromagnetic spectrum, are available for determination of solar abundances. At optical wavelengths, photospheric abundances can be determined from the “equivalent widths” of the Fraunhofer absorption lines of neutral, singly, and doubly ionized atoms (Athay 1986). Chromospheric and low corona abundances may be determined from observations of permitted UV emission lines from various ionization stages (Pottash 1964; Mariska 1980; Widing & Feldman 1989). Coronal abundances have been derived from the analyses of the solar X-ray and EUV spectra (Parkinson 1977; Veck & Parkinson 1981; Feldman 1992) or from optically forbidden emission lines of highly ionized species (Mason 1975; Arnaud 1984). In situ studies using spacecraft measurements have been made for the elemental composition of the solar wind (Geiss 1982; Geiss & Bochsler 1986) and solar energetic particles (Meyer 1985a, 1985b; McGuire, von Rosevinge, & McDonald 1985; Stone 1989). Spectroscopic X-ray and EUV research over the past 10 years strongly indicates that the elemental abundances in the solar corona differ from photospheric values (Feldman 1992; Meyer 1993). The compositional differences may be organized in terms of the first ionization potential (FIP). Elements with FIP less than 10 eV were observed to be more abundant in the corona (by up to an order of magnitude), with the abundance varying from time to time and from coronal structure to structure.

For investigations that are made in the X-ray or EUV, there are several considerations: (1) the line intensities must be accurately determined, (2) the atomic data must be accurately known in order to calculate the synthetic spectra which are fitted to the observations, and (3) the conditions of the emitting solar plasma with regard to various assumptions such as thermal equilibrium must be evaluated. It is relatively easy to accommodate for these considerations in the analysis of X-ray or EUV spectra, contrary to the analysis of spectra from the visible range.

In an earlier analysis on a limited set of data from the NASA *Solar Maximum Mission* (SMM) (Sylwester, Lemen, & Mewe 1984; Lemen, Sylwester, & Bentley 1986; Fludra et al. 1991), we were the first to point out the presence of flare-to-flare variations of A_{Ca} from spectroscopic studies. More recent analyses of calcium data were done by Fludra et al. (1993) and Bentley, Sylwester, & Lemen (1998), who derived A_{Ca} using data from the crystal spectrometer on the Japanese *Yohkoh* satellite, and Sterling, Doschek, & Feldman (1993), who studied data obtained with the SOLFLEX instrument on P78-1. In order to obtain absolute abundances, the latter authors normalized their results to the SMM–Bent Crystal Spectrometer continuum observations. In this work, observations of the line and continuum obtained with the same spectrometer are analyzed.

In this paper, we present a method of determining the absolute calcium abundance relative to hydrogen using the data acquired from flare plasmas observed with the Bent Crystal Spectrometer (BCS) on board SMM. The SMM-BCS was one of two spectrometers constituting the X-Ray Polychromator experiment (Acton et al. 1980). We investigate the flare-to-flare variations of the Ca XIX resonance line (w) intensity, $^1S_0-^1P_1$ at 3.178 Å, relative to the nearby continuum (Veck & Parkinson 1981; Sylwester et al. 1984). The values of A_{Ca} are determined for 146 flares during the decay phase. Contrary to the case for photo-

¹ Current affiliation: Rutherford Appleton Laboratory, Astrophysics and Geophysics Division, Chilton, Didcot, Oxfordshire OX11 0QX, United Kingdom.

spheric abundance studies, coronal abundances are generally not measured relative to hydrogen; only ratios of heavy elemental abundances are normally obtained. The only way to measure the ratio of heavy elemental abundances relative to H is to make use of the line-to-continuum ratio. The Ca XIX *w* line is a particularly good choice for abundance determinations because the intensity ratio of this line relative to the nearby continuum varies only weakly with temperature; thus, estimates of abundance may be reliably obtained within the isothermal approximation. The Ca XIX line is very bright in solar flare spectra, and so its intensity can be easily measured. Theoretical calculations are available for the complex of Ca XVIII–XIX near $\lambda = 3.2$ Å. The spectral fitting makes use of a semiempirical determination of the Ca XIX fractional ionization as derived by Lemen et al. (1998).

2. THE BENT CRYSTAL SPECTROMETER

The BCS is one of two X-ray spectrometers that make up the X-Ray Polychromator (XRP) instrument. The SMM-BCS consists of a collimator, eight curved germanium crystals, eight one-dimensional position-sensitive sealed proportional counters, detector amplifiers, and processing and control electronics. The multigrad collimator had a $6' \times 6'$ FWHM triangular response in two directions, parallel and perpendicular to the dispersion axis; the dispersion axis was parallel to the east-west direction on the Sun. The collimator resolution is sufficient to isolate the field of view to an individual active region on the Sun. The observing target was selected by pointing the SMM spacecraft using ground control commands.

The SMM-BCS observed the helium-like Ca XVIII–XIX lines near 3.2 Å in one channel and various highly ionized iron transitions near $\lambda = 1.9$ Å in the other seven channels. A typical calcium flare spectrum is shown in Figure 1. The principal lines are labeled: the resonance line ($1s^2\ ^1S_0-1s2p\ ^1P_1$) as *w*, the intercombination lines ($1s^2\ ^1S_0-1s2p\ ^3P_{1,2}$) as *y* and *x*, and the forbidden line ($1s^2\ ^1S_0-1s2p\ ^3S_1$) as *z*.

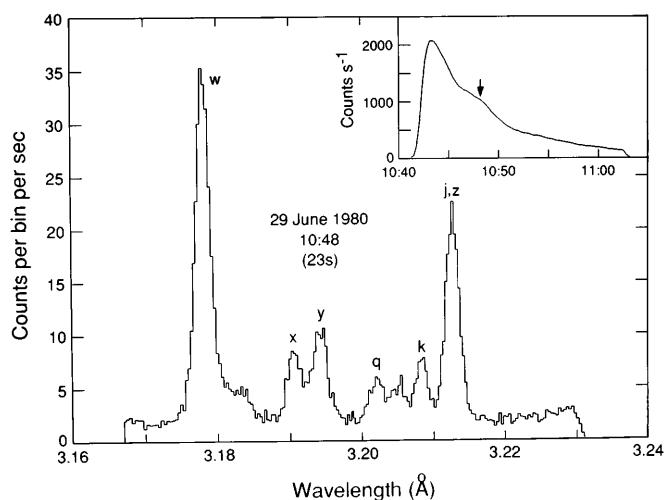


FIG. 1.—Example of a Ca XVIII–XIX spectrum recorded by SMM-BCS from the decay phase of the flare on 1980 June 29 at 10:48 UT; the integration time was 23 s. The minimum threshold for detection with this spectrometer is $T > 7$ MK, $EM > 5 \times 10^{47} \text{ cm}^{-3}$. The principal line features are labeled and explained in the text. The thermal continuum is seen at the short wavelength side of the resonance line and longward of the *j*, *z* line complex. The insert shows the time history of the count rate integrated over all wavelengths for this flare, and the arrow marks the time of the displayed spectrum.

Besides these main spectral features, numerous blended satellite lines [e.g., *k*, $1s^2 2p^2 P_{1/2}-1s2p^2 D_{3/2}$; *q*, $1s^2 2s^2 S_{1/2}-1s2p(^1P)2s^2 P_{3/2}$] contribute to the observed spectrum. Low background count rates together with high spectral resolution ($\lambda/\delta\lambda \approx 3450$) permit the accurate determination of the line and continuum fluxes.

The solar X-rays that enter the SMM-BCS through the multigrad collimator are dispersed by eight curved, germanium crystals (each approximately 15 cm long and 2.5 cm wide) into position-sensitive sealed proportional counters. The Ca XIX channel (channel 1) made use of the Ge 220 crystal plane. Because the crystals are curved, there are no moving parts in the spectrometer, but rather X-rays are dispersed along the position-sensitive proportional counters according to the Bragg diffraction condition:

$$\lambda = 2d \sin \theta, \quad (1)$$

where $2d$ is the crystal spacing and λ is the wavelength of the radiation refracted at the angle θ . Because the crystal is curved, the Bragg condition is satisfied for different wavelengths along the length of the crystal. The position at which a photon is detected in the proportional counter is related to its incident energy.

This type of spectrometer provides an advantage over spectrometers that scan a flat crystal if the spectra evolve rapidly, as during a solar flare. The SMM-BCS observes at all wavelengths simultaneously, and so there are no uncertainties about spectral evolution during the acquisition of a spectrum as there might be if the crystal is scanned over a range of wavelengths. The SMM-BCS has high sensitivity (effective area = 0.024 cm²), and relatively short integration periods, of the order of tens of seconds, are required to obtain statistically acceptable spectra.

The Ca XIX channel proportional counter had a 75 μm thick beryllium window and was filled with a mixture of noble gases. The average background level due to energetic particles was low, always less than 0.03 counts per wavelength bin per second, normally less than 1% of the observed continuum. During flight, Fe⁵⁵ X-ray calibration sources were routinely exposed to the SMM-BCS detectors to monitor detector gain, and additional functional tests were carried out on a routine basis to monitor the linearity of the signal processing chain. All standard corrections resulting from the calibration data acquired in orbit have been applied to the SMM-BCS spectra in the course of our analyses.

In the other SMM-BCS wavelength channels, an enhanced background is observed, contaminating the continuum, especially during the rise phase of flares. This is caused by the fluorescence of the germanium crystals by solar X-rays whose energies exceed the 11.1 keV ionization threshold of germanium (Parmar et al. 1981). Fortunately, the calcium spectrometer channel is free from this problem, since the pulse height discrimination of the processing electronics rejected all high-energy, nonsolar flux.

The SMM-BCS instrument operated during 1980 February–November in the first year of SMM operations and then again for several more years (1984–1989) following the in-orbit repair of the spacecraft.

3. THE LINE-TO-CONTINUUM RATIO

The spectrum in the vicinity of Ca XIX, He-like X-ray triplet lines (resonance *w*, intercombination *x*, *y*, and forbidden *z*) includes blends of hundreds of satellite lines in

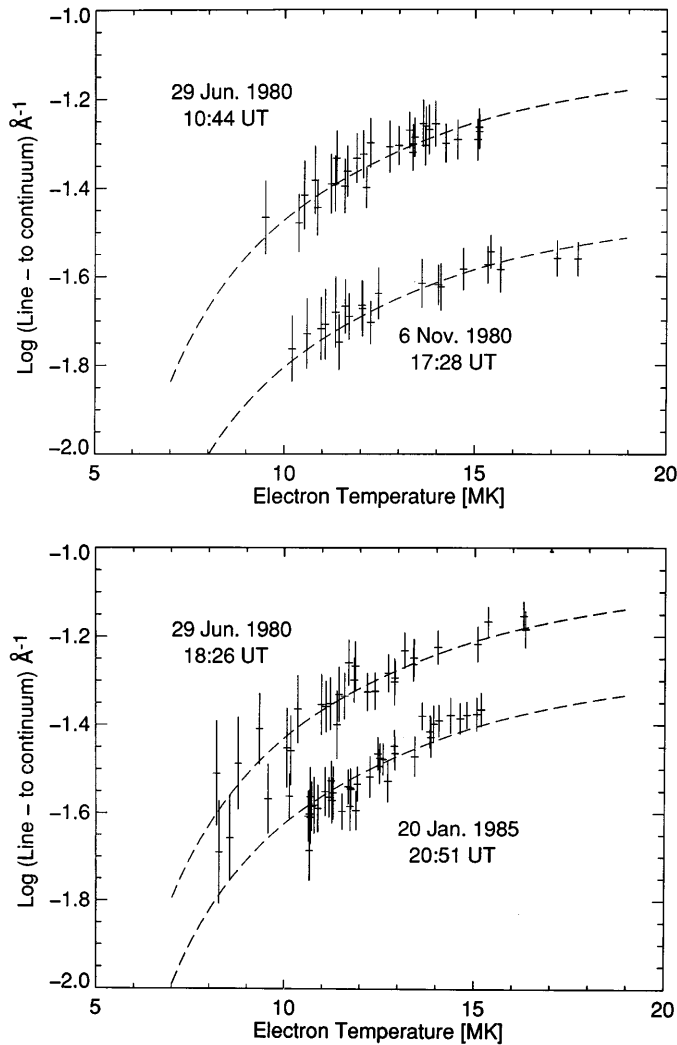


FIG. 2.—Examples of F_w/F_c vs. T dependence are shown for two pairs of flares with substantially different line-to-continuum values. Error bars indicate $\pm 1 \sigma$ uncertainties as determined from the least-squares spectral fitting procedure. As this data is taken from the flare decay, the time ordering of the data generally is from right to left in these figure panels.

Ca XVIII (see Fig. 1). The upper states of the triplets are largely populated by direct excitation with some contributions from radiative recombination. The satellites are formed by inner shell excitation and dielectronic recombination.

The photon flux for the calcium resonance emission can be shown to be optically thin for the case of the corona (see § 6.2). The flux at the Earth (photon $\text{cm}^{-2} \text{s}^{-1}$) in the emission line can be expressed as (Sylwester, Schrijver, & Mewe 1980b)

$$F_i = A_{\text{Ca}} \int f_i(T) \varphi(T) dT, \quad (2)$$

where $\varphi(T)$ is the distribution of the emission measure over the temperature (differential emission measure) in the source. A_{Ca} is the abundance (relative to hydrogen) of calcium. The abundance is assumed to be uniform in the emitting region. The emission functions $f_i(T)$ can be expressed as

$$f_i(T) = (3.0 \times 10^{-28}) \frac{N_e}{N_H} \frac{N_i}{N_{\text{Ca}}} \xi_i(T), \quad (3)$$

where N_e and N_H are the electron and hydrogen number densities, respectively; $N_e/N_H = 0.85$ is assumed, which is appropriate for a fully ionized solar plasma. The effective excitation rates $\xi_i(T)$ are taken from the calculations of Bely-Dubau et al. (1982), who take into account contributions from higher n satellite transitions. The ionization fraction is given by N_i/N_{Ca} . We use values for $N_{\text{CaXIX}}/N_{\text{Ca}}$ derived by Lemen et al. (1998) from semiempirical fits to SMM-BCS flare spectra.

The photon flux per unit wavelength interval in the continuum can be expressed as

$$F_c = \int f_c(\lambda, T) \varphi(T) dT, \quad (4)$$

where the emission function $f_c(\lambda, T)$ for the continuum has been taken from Mewe et al. (1986), who assume standard cosmic abundances of Allen (1973). Values of the continuum emission function depend only weakly on the plasma composition (see discussion in § 6.4).

The ratio of the w resonance line flux to the continuum at the wavelength of this line, $\lambda_w = 3.178 \text{ \AA}$, can be calculated from equations (2) and (4), assuming an isothermal plasma, as

$$F_w/F_c = A_{\text{Ca}} f_w(T)/f_c(\lambda_w, T), \quad (5)$$

where $f_c(\lambda_w, T)$ is the continuum flux at the wavelength of the Ca XIX w line. The ratios of F_w/F_c are shown as dashed curves in Figure 2, where the value of A_{Ca} has been adjusted to fit the observations. One can see from the plot that F_w/F_c varies by about a factor of 3 over the range of typical flare temperatures (8–20 MK). The relatively weak temperature dependence of this ratio means that errors in the temperature estimates of the spectra will introduce only a small uncertainty in the estimates for the calcium abundance. Furthermore, a weak dependence on temperature means that the introduction of an isothermal assumption will result in only a small error for the abundance determination (see § 6.5).

4. OBSERVATIONS

This study includes bright flares that were observed with the SMM-BCS in 1980, the first year of SMM operations, and during 1984–1987, the years following the in-orbit repair of the spacecraft. Flares in 1980 were selected from events whose integrated Ca XIX light curves had maximum count rates at the peak of the flare that were greater than 80 counts s^{-1} . During the postrepair mission period (1984–1987), flares listed in the XRP Team Final Report (Strong 1988) were selected that had greater than 100 counts s^{-1} at flare maximum. This criterion resulted in the identification of more than 250 flares. Some flares were subsequently eliminated because of data gaps.

The present paper concentrates on flare decay phase data. There are several reasons for this. Generally, most flares as observed in hard and soft X-rays are seen to have a prompt energy release, sometimes accompanied by the acceleration of fast particles. In hard X-rays, the emission often appears to be nonthermal and intensity increases are often impulsive. During the decay phase, there is usually no hard X-ray emission, indicating that flare heating has ceased or is greatly reduced. As a result, the ionization state of the plasma is quasi-stationary (§ 6.3) and plasma densities are higher, so one may neglect effects of transiently ionizing

plasma. An isothermal approximation is also better during the decay phase. The absence of intense hard X-ray emission with energies greater than 11.1 keV lessens the danger of contamination of the thermal continuum from fluorescence of the germanium crystals. The continuum is assumed to be thermal and not a mixture of thermal and nonthermal emission.

As the intrinsic line widths of the considered calcium transitions under low plasma density conditions are very small, the observed line widths are mainly determined by four factors: Doppler broadening, the instrument response function, the physical source size within the BCS field of view, and nonthermal plasma motions. The Doppler broadening is assumed to be Gaussian and is treated as a free parameter during the fitting procedure. The instrument spectral response function is characterized as a Voigt profile with corresponding Gaussian (FWHM = 0.527 mÅ) and Lorentzian (FWHM = 0.612 mÅ) components. The source size is limited by the actual flare size, which is generally much less than the size of the BCS collimator (FWHM = 6' × 6'). During the decay phase, the nonthermal widths are small and directed flows are small (Fludra et al. 1989), which simplifies the line fitting. The observed line widths during the flare decay are dominated by Doppler broadening convolved with the instrumental response. Broadening due to other effects are less significant, but their possible presence has been accommodated by including an additional symmetric Gaussian component in the fitting process.

From the original set of over 250 flares, 146 flares with good data during the decay phase were fitted to measure the line-to-continuum values. Included in our sample are 28 flares that were analyzed by Lemen et al. (1998) in order to determine a semiempirical value for the ionization fraction of $N_{\text{CaXIX}}/N_{\text{Ca}}$. More than 5000 spectra were fitted in total. Each spectral fit was examined visually, and unsatisfactory cases were eliminated from the analysis.

5. CALCIUM ABUNDANCE RESULTS

The calcium abundance was determined by fitting the theoretical value of the line-to-continuum ratio, F_w/F_c , to the line-to-continuum observed during the decay phases of our set of flares. The value of the resonance line intensity, F_w , and the continuum flux at line w are obtained in the following manner. First, the spectrum is fitted with a complete spectral model, including all line blends and nearby satellites, in order to determine the best value of the electron temperature T and the isothermal emission measure. Under the assumption of an isothermal plasma, the emission measure $\int \phi(T)dT$ becomes $\text{EM} = \int N_e^2 dV$, where $\int dV$ is the volume of the emitting plasma. Values of F_w/F_c were computed (eq. [5]) from the fitted T and EM results, assuming for consistency the same A_{Ca} that was used in the fit. By these means, the intensity of F_w itself can be estimated without the contribution of the nearby dielectronic satellites. Systematic uncertainties in our derived theoretical values for F_w/F_c will lead at most to 20% errors in the estimated values of A_{Ca} (Lemen et al. 1998). In our synthetic model, the theoretical spectra were convolved through the SMM-BCS instrument response function. The fitting code fits the resonance line (w) and wavelength region near the dielectronic satellite line (k). Further discussions about the fitting approach are given in Lemen et al. (1998), Fludra et al. (1989), and Lemen et al. (1984). The results of our fitting

program have been compared with Antonucci et al. (1982), who use the same atomic data and are shown to be in relatively good agreement, except that the temperature values obtained by Antonucci et al. (1982) appear to be systematically lower by ~ 1 MK. This is probably caused by the different method of fitting spectra used by Antonucci et al. and their assumption that the thermal continuum is approximated as a constant in wavelength over the limited range of the SMM-BCS calcium spectrometer. In our fitting algorithm, the continuum spectrum is explicitly computed and a least-squares fitting method is used to choose the best-fit parameters. However, the small difference in the estimated temperatures from the two fitting methods is not significant in terms of the present analysis, and the use of the Antonucci et al.'s results would have resulted in substantially the same estimates for the A_{Ca} .

The derived F_w/F_c values are shown for four flares in Figure 2 as data points. The values of F_w/F_c are plotted as a function of electron temperature T , and thus the time order of the measurements generally proceeds from right to left in the plot. The error bars represent 1σ uncertainties that are derived from the estimates of the goodness of fit by the spectral fitting code. The F_w/F_c curves for the two flares in the upper panel, observed on 1980 June 29 at about 10:44 UT and 1980 November 6 at about 17:28 UT, differ by a factor of about 2, although their shapes as a function of temperature follow a similar trend. From equation (5), one interpretation for this behavior is that the calcium abundance relative to hydrogen is different for the two cases. The values of A_{Ca} are estimated by fitting the predicted F_w/F_c to the observed F_w/F_c . The dashed curves are the best-fit values of F_w/F_c , where the value of A_{Ca} has been allowed to vary. The fits result in $A_{\text{Ca}} = (7.30 \pm 0.16) \times 10^{-6}$ for 1980 June 29 at 10:44 UT and $A_{\text{Ca}} = (3.40 \pm 0.09) \times 10^{-6}$ for the flare on 1980 November 6 at 17:28 UT. The uncertainties in the measurements of the abundances come from the fits of the observed values of F_w/F_c to the theoretical values. These errors take into account both the uncertainties of temperature and continuum level determinations (see Lemen et al. 1998). The lower panel in Figure 2 gives two more examples of flares with significantly different line-to-continuum values. The upper set of data was also taken from 1980 June 29 but from a flare that occurred later in the day at 18:26 UT, and the lower data set is for the flare that occurred on 1985 January 20 at 20:51 UT. The derived values of A_{Ca} for these two flares are $(8.06 \pm 0.17) \times 10^{-6}$ and $(5.15 \pm 0.08) \times 10^{-6}$, respectively. Note that the uncertainties in the individual abundance measurements are much smaller than the flare-to-flare variations for these cases.

In this analysis, it has been assumed that the calcium abundance remains constant during the decay phase of each flare. This assumption appears to be justified by the fact that a comparison of many flares shows that most flares have approximately the same shape of observed F_w/F_c as a function of temperature (see Lemen et al. 1998 for more details). In some cases, one or more additional heating episodes are observed during the decay phase; these cases are treated as separate flares.

When comparing flares with widely different abundances, it is possible to visually identify the difference in the spectra. Figure 3 shows two spectra taken from the flares shown in Figure 2, plotted as histograms. The solid curves superposed on the observed spectra are the best-fit synthetic

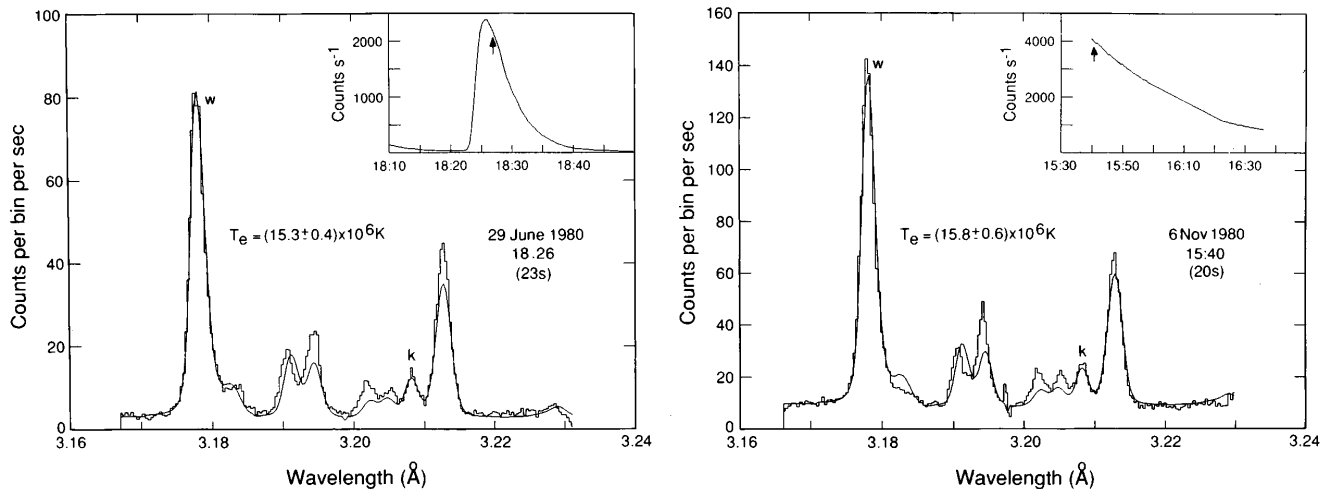


FIG. 3.—Comparison of two spectra observed for flares with significantly different F_w/F_c ratios. The solid curves superposed on the observed spectra are the best-fit synthetic spectra. The spectral fitting routine adjusts the electron temperature to match the temperature-sensitive intensity ratio of the dielectronic satellite line k to the resonance line w to the observed spectrum. These two spectra have nearly the same fitted electron temperatures and line widths. Note the different values of the w line-to-continuum ratio that are seen for these two spectra. The inset is as in Fig. 1.

spectra. These two spectra were chosen because their fits resulted in nearly the same electron temperatures and line widths. The plot shows the different resonance line-to-continuum ratios for these two flares.

Table 1 summarizes the results for 146 flare decay phases. Included in the table is the NOAA active region number, the location on the solar disk of the flare, $H\alpha$ and *GOES* X-ray flare classifications, and number of spectra included in the determination of each abundance estimate. The values of A_{Ca} have been multiplied by 10^6 to facilitate the display in the table. The values labeled $\pm 1\sigma$ are the uncertainties that were described above. The times given represent the approximate peak of the flares as observed in the *SMM*-BCS. The average abundance for all 146 flare decay

phases is $(5.77 \pm 1.41) \times 10^{-6}$. This is greater than the typically quoted photospheric value of $A_{Ca} = (2.6 \pm 0.4) \times 10^{-6}$ or the coronal value determined by Veck & Parkinson (1981) of $A_{Ca} = (3.2 \pm 1.2) \times 10^{-6}$ but is similar to the value of 5×10^{-6} of Sterling et al. (1993).

The variation in the values of A_{Ca} is much larger than the typical errors of the abundance determination, which supports the hypothesis that the *SMM*-BCS observations demonstrate flare-to-flare variations in the coronal calcium abundance. Figure 4 shows a histogram distribution of the results organized according to abundance value. The width of each bin is chosen to be approximately equal to the average root mean square (rms) uncertainty for determination of the A_{Ca} . The differently hatched areas correspond to subsets of flares from two active regions: Active Region 2779 and Active Region 4474. The width of the distribution for entire sample is much larger than the rms error for determining the abundance for a given flare. In case of the flares observed from AR 2779 and AR 4474, the distribution of A_{Ca} is narrower than for the entire sample and their centroids differ substantially.

6. DISCUSSION

A major result of this analysis is the finding of a systematic flare-to-flare variation in the Ca XIX line-to-continuum ratio during the decay phases of flares, which we interpret as a variation in the coronal calcium abundance. Meyer (1985a, 1985b) pointed out that the abundances of low-FIP elements (less than 10 eV, such as calcium) are larger in the corona compared to the photosphere. As mentioned by Sterling et al. (1993), this suggests that the composition of the solar corona depends upon some mechanism that is acting on the ionized plasma, although there is no generally accepted mechanism to explain this phenomenon. The present results suggest that the situation is even more complicated and that the mechanism responsible for the variation of A_{Ca} for different flares is time- and active region-dependent.

Solar cycle effects were investigated by comparing the average abundances recorded from flares observed in a single active region. Only active regions with four or more flares observed were considered. Table 2 shows the average

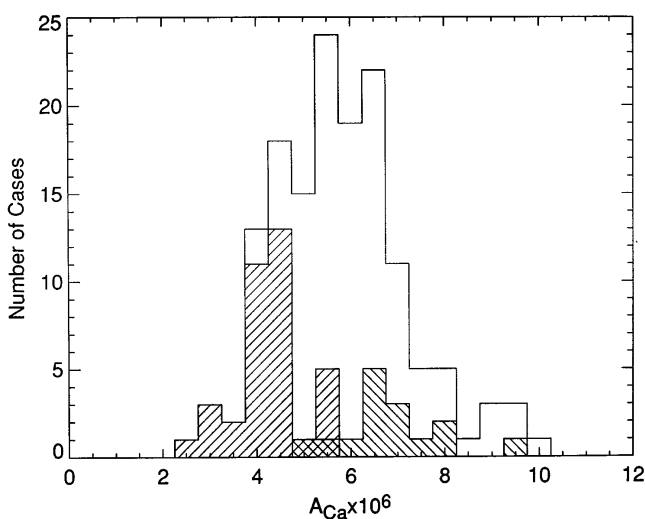


FIG. 4.—Distribution of calcium abundance estimates for the studied flares. The width of a histogram bin corresponds approximately to the mean rms uncertainty for an individual abundance estimate. The width of the A_{Ca} distribution is over 6 times greater than the average uncertainty for a single abundance estimate and indicates a substantial variation in the calcium composition—by over a factor of 3.5—between flares. A systematic uncertainty of up to 20% may be assigned to the abundance scale. Differently hatched areas correspond to distributions of A_{Ca} for flares from active regions AR 2779 (at lower values) and AR 4474 (at higher values).

TABLE 1
ABSOLUTE CALCIUM ABUNDANCES A_{Ca} FOR ANALYZED FLARES

Date/UT (1)	Active Region Number (2)	Location (deg) (3)	H α (4)	GOES (5)	$A_{\text{Ca}} \pm 1 \sigma$ (6)	N (7)
1980 Apr 7/01:08	2372	N10, E03	1B	M4	5.70 ± 0.09	45
1980 Apr 7/05:41	2372	N12, E01	1B	M8	5.51 ± 0.07	59
1980 Apr 8/03:07	2372	N12, W13	1B	M4	6.49 ± 0.12	32
1980 Apr 10/09:22	2372	N12, W42	1N	M4	6.82 ± 0.16	30
1980 Apr 13/04:08	2372	N10, W77	1F	M1	6.44 ± 0.16	49
1980 Apr 30/20:25	2396	S13, W90	SN	M2.2	6.22 ± 0.15	26
1980 May 7/14:57	2418	S22, W12	SB	C7	7.30 ± 0.51	9
1980 May 9/07:15	2418	S21, W32	1B	M7.2	6.37 ± 0.10	32
1980 May 21/21:05	2456	S14, W15	2B	X1.4	5.94 ± 0.07	58
1980 Jun 4/09:11	2490	S13, E58	SB	M4	7.09 ± 0.10	85
1980 Jun 13/22:34	2502	N17, E11	1B	...	6.21 ± 0.46	7
1980 Jun 21/01:02	2528	S12, E17	2N	M2	5.79 ± 0.11	51
1980 Jun 24/15:24	2522	S29, W15	SB	M1	6.27 ± 0.26	11
1980 Jun 25/15:55	2522	S29, W28	1B	M4.8	6.43 ± 0.33	5
1980 Jun 29/02:38	2522	S27, W90	...	M3.6	6.91 ± 0.14	36
1980 Jun 29/10:44	2522	S27, W90	1F	M4.2	$7.30, 0.16$	32
1980 Jun 29/18:26	2522	S20, W90	SN	M4.2	8.06 ± 0.17	32
1980 Jul 1/16:28	2544	S12, W38	1B	X2.5	6.72 ± 0.14	29
1980 Jul 5/22:45	2550	N28, W31	1B	M8.9	5.62 ± 0.05	97
1980 Jul 7/11:53	2550	N26, W49	SB	M2	7.91 ± 0.40	11
1980 Jul 11/22:18	2562	S10, E70	2B	M5.3	5.47 ± 0.13	55
1980 Jul 12/11:21	2562	S14, E56	SB	M4.3	6.91 ± 0.15	60
1980 Jul 12/16:00	2562	S10, E60	1B	M3.2	6.86 ± 0.39	19
1980 Jul 12/17:38	2562	S09, E59	SB	C7	5.90 ± 0.54	8
1980 Jul 12/19:25	2562	S12, E60	SN	C5	6.01 ± 0.98	5
1980 Jul 12/19:33	2562	S14, E53	1F	C4	6.55 ± 0.99	5
1980 Jul 13/06:33	2562	S13, E48	SN	C4	7.98 ± 0.57	14
1980 Jul 13/14:34	2562	S15, E49	SB	C6	7.50 ± 0.77	6
1980 Jul 13/17:33	2562	S10, E46	SB	M2	6.74 ± 0.37	20
1980 Jul 13/18:03	2562	S09, E49	SB	C6	9.14 ± 0.75	6
1980 Jul 13/19:19	2562	S13, E50	SB	C9.2	6.95 ± 0.50	8
1980 Jul 13/19:22	2562	S13, E50	SB	C9.2	6.40 ± 0.59	3
1980 Jul 13/19:32	2562	S13, E50	SB	C9.2	8.86 ± 0.71	10
1980 Jul 14/01:52	2562	S10, E43	SN	C4.7	6.56 ± 0.78	5
1980 Jul 14/08:27	2562	S13, E43	1B	X1.1	5.88 ± 0.18	16
1980 Jul 15/22:48	2562	S15, E18	SB	C4.4	5.74 ± 0.94	4
1980 Jul 17/06:11	2562	S12, E06	1B	M3.4	5.23 ± 0.08	88
1980 Jul 20/19:26	2562	S19, W45	1B	M1.4	5.84 ± 0.41	6
1980 Jul 21/03:00	2562	S14, W60	1B	M8	7.32 ± 0.27	13
1980 Aug 23/21:30	2629	N16, W39	1B	M2.1	5.34 ± 0.45	23
1980 Aug 24/16:12	2629	N17, W52	SB	M1	6.31 ± 0.27	19
1980 Aug 24/16:35	2629	N17, W52	SB	...	5.77 ± 0.70	7
1980 Aug 25/13:05	2629	N18, W62	SB	M1	5.70 ± 0.16	45
1980 Aug 31/12:49	2646	N12, E28	SB	...	8.88 ± 0.47	7
1980 Aug 31/12:52	2646	N12, E28	SB	M2.8	6.03 ± 0.66	5
1980 Aug 14/06:14	2725	S09, W07	3B	X3.3	4.21 ± 0.05	50
1980 Oct 20/18:34	2744	S17, E45	SN	M1.0	5.17 ± 0.29	8
1980 Nov 5/22:29	2776	N11, E07	4.26 ± 0.14	8
1980 Nov 5/22:34	2776	N10, E07	1B	M4.0	4.52 ± 0.31	7
1980 Nov 6/10:12	2779	S11, E71	SF	C7	4.17 ± 0.32	3
1980 Nov 6/11:25	2779	S13, E66	1F	C7	2.94 ± 0.18	8
1980 Nov 6/11:45	2779	S12, E66	SF	C9	2.56 ± 0.26	2
1980 Nov 6/12:36	2779	S09, E65	...	M3.1	2.78 ± 0.12	13
1980 Nov 6/14:13	2779	S09, E65	...	M3.1	3.46 ± 0.15	9
1980 Nov 6/15:26	2779	S09, E65	2B	X1.2	4.24 ± 0.04	86
1980 Nov 6/17:28	2779	S09, E65	2B	M4.2	3.40 ± 0.09	21
1980 Nov 7/04:47	2779	S11, E57	4.03 ± 0.07	41
1980 Nov 7/04:58	2779	S11, E57	SN	M2.5	3.92 ± 0.18	8
1980 Nov 7/09:41	2779	S06, E59	SB	M1.2	4.76 ± 0.24	12
1980 Nov 7/11:37	2779	S11, E50	SN	M1.0	4.66 ± 0.21	14
1980 Nov 7/14:41	2779	S07, E56	SB	M4	3.84 ± 0.23	8
1980 Nov 7/15:35	2779	S07, E56	SB	...	4.00 ± 0.35	3
1980 Nov 7/15:37	2779	S07, E56	SB	C7.6	3.91 ± 0.81	2
1980 Nov 7/15:39	2779	S07, E56	SB	C7.6	3.17 ± 0.31	3
1980 Nov 7/22:30	2779	S10, E47	1N	M1	4.36 ± 0.07	62
1980 Nov 8/11:26	2779	S15, E43	SB	C6.2	4.50 ± 0.36	6
1980 Nov 8/16:19	2779	S08, E42	SN	C4.9	4.28 ± 0.41	2
1980 Nov 9/04:30	2779	S09, E36	SB	M1	4.54 ± 0.23	15

TABLE 1—Continued

Date/UT (1)	Active Region Number (2)	Location (deg) (3)	H α (4)	GOES (5)	$A_{Ca} \pm 1 \sigma$ (6)	N (7)
1980 Nov 9/17:21	2779	S11, E21	SN	C5.3	3.92 ± 0.21	8
1980 Nov 10/08:12	2779	S12, E14	1B	M1.4	4.37 ± 0.11	19
1980 Nov 10/09:37	2779	S15, E11	1F	M1.5	4.05 ± 0.11	29
1980 Nov 11/06:29	2779	S12, E06	SN	M1.2	4.69 ± 0.24	8
1980 Nov 11/10:32	2779	S12, E02	1N	M3.6	4.70 ± 0.47	3
1980 Nov 11/15:17	2779	S12, W01	1B	M1	5.37 ± 0.46	14
1980 Nov 11/15:54	2779	S12, W01	SB	M2	4.50 ± 0.14	13
1980 Nov 12/02:51	2779	S13, W06	1B	M1.9	4.66 ± 0.11	45
1980 Nov 12/08:10	2779	S12, W10	...	C8	4.01 ± 0.23	5
1980 Nov 12/09:24	2779	C8	3.79 ± 0.35	3
1980 Nov 12/11:06	2779	S12, W10	1F	C8.6	5.49 ± 0.33	18
1980 Nov 12/17:04	2779	S14, W11	1B	M1.4	5.27 ± 0.37	14
1980 Nov 12/17:37	2779	S13, W15	SN	C7	4.52 ± 0.25	10
1980 Nov 12/23:35	2779	S13, W18	1B	M3	4.29 ± 0.24	5
1980 Nov 13/01:03	2779	S11, W21	1B	M9.4	4.38 ± 0.06	85
1980 Nov 18/14:55	2779	S10, W90	SB	M3.0	5.64 ± 0.13	29
1980 Nov 19/05:44	2779	S10, W90	...	M6.0	5.26 ± 0.10	32
1980 Nov 22/05:38	2793	N12, W02	2N	C9.0	4.82 ± 0.26	10
1984 Apr 25/00:22	4474	S12, E43	3B	X10	5.99 ± 0.14	10
1984 Apr 25/00:57	4474	S11, E42	2F	...	5.28 ± 0.08	69
1984 Apr 26/09:03	4474	S09, E34	1B	M2.5	7.02 ± 0.17	20
1984 Apr 27/05:40	4474	S10, E24	SB	M2.3	5.04 ± 0.19	9
1984 Apr 29/02:50	4474	S13, E12	SN	C4.8	6.61 ± 0.24	39
1984 Apr 29/07:44	4474	S17, E02	1N	M1	9.39 ± 0.57	9
1984 Apr 30/05:57	4474	S14, W34	1B	M1.1	6.88 ± 0.20	41
1984 Apr 30/12:13	4474	S12, W31	2B	M2.3	7.47 ± 0.20	64
1984 May 1/01:34	4474	S14, W32	2B	M4.0	6.70 ± 0.10	96
1984 May 2/16:17	4474	S14, W54	SB	C7.9	6.58 ± 0.20	31
1984 May 2/19:25	4474	S11, W58	SB	M3.0	6.31 ± 0.10	37
1984 May 2/20:23	4474	6.73 ± 0.40	22
1984 May 2/20:58	4474	6.99 ± 0.43	18
1984 May 3/03:18	4474	S12, W67	SB	C7.1	7.83 ± 0.34	18
1984 May 5/01:07	4476	S11, W64	SF	C4.7	8.38 ± 0.53	12
1984 May 5/18:24	4474	S11, W90	...	M7.5	7.84 ± 0.10	31
1984 May 6/01:45	4481	N06, E83	SF	C5	9.60 ± 0.68	11
1984 May 6/08:23	4481	N07, E89	SB	C3	5.58 ± 1.36	2
1984 May 6/16:25	4481	N08, E89	SB	C3.1	10.2 ± 1.44	3
1984 May 6/19:04	4481	N05, E78	SN	C3.8	9.44 ± 0.59	11
1984 May 19/21:55	4492	S10, E66	2B	X4.1	3.93 ± 0.04	65
1984 May 20/01:29	4492	S10, E64	1B	M2.9	6.64 ± 0.13	38
1984 May 20/03:01	4492	S13, E62	SB	M4.6	6.33 ± 0.10	40
1984 May 20/03:02	4492	S13, E62	SB	M4.6	5.01 ± 0.32	9
1984 May 20/05:42	4492	S08, E57	1B	M5.4	6.20 ± 0.12	35
1984 May 20/22:53	4492	S08, E52	2B	X10	5.35 ± 0.10	47
1984 May 20/23:11	4492	S06, E53	SN	X10.	4.76 ± 0.09	22
1984 May 21/17:47	4492	S06, E42	1N	...	6.06 ± 0.29	14
1984 May 21/18:10	4492	S08, E42	1B	C9.7	5.43 ± 0.12	24
1984 May 22/15:01	4492	S09, E24	2B	M6.3	5.19 ± 0.13	15
1985 Jan 20/20:51	4617	S09, W24	1B	M4.1	5.15 ± 0.08	40
1985 Jan 21/03:53	4617	S10, W28	SN	M2.2	4.95 ± 0.13	15
1985 Jan 21/14:19	4617	S09, W35	SN	M2.4	6.80 ± 0.41	14
1985 Jan 23/07:33	4617	S10, W56	1N	...	6.01 ± 0.31	9
1985 Jan 23/07:43	4617	S11, W58	1N	M1.3	5.86 ± 0.21	11
1985 Jan 23/07:52	4617	S11, W58	1N	M1.3	6.94 ± 0.39	6
1985 Apr 24/01:52	4647	N05, E26	1N	C8.8	6.32 ± 0.23	14
1985 May 2/08:19	4647	N03, W86	1B	...	6.11 ± 0.12	60
1985 May 21/09:55	4656	N05, E27	SN	...	5.54 ± 0.53	3
1985 Jul 2/21:26	4671	S14, E57	2B	M4.5	6.75 ± 0.10	39
1985 Jul 7/05:28	4671	S15, E00	SN	C3.0	4.29 ± 0.44	3
1985 Jul 7/20:28	4671	C2.7	5.87 ± 0.61	3
1985 Jul 9/02:10	4671	S13, W25	1N	...	5.60 ± 0.27	8
1985 Jul 13/06:59	4671	S17, W86	SN	C2.3	5.76 ± 0.50	3
1985 Jul 13/13:21	4671	C2.0	6.23 ± 0.64	2
1985 Oct 26/04:34	4698	N06, W58	1N	M1.8	6.46 ± 0.25	23
1986 Oct 7/10:56	4711	S11, W21	2B	M5.2	5.75 ± 0.16	18
1986 Oct 19/00:46	4750	N23, E62	2N	M4.7	5.61 ± 0.23	9
1986 Oct 19/01:41	4750	N23, E62	2N	M4.7	6.28 ± 0.17	32
1986 Oct 24/12:40	4750	...,...	...	C2.4	4.99 ± 0.68	3
1987 Apr 5/19:37	4787	S29, E90	SN	M1.1	4.99 ± 0.51	3

using a standard statistical analysis. The values represent the probabilities that two active regions are not distinguishable. Thus, low values indicate that the average abundances for the paired active regions are significantly different. The table shows that there is a low probability of a chance occurrence of similar values of average A_{Ca} between the paired active regions in most cases. The active region that has the largest difference from any other is AR 2779, and the flares with the smallest abundance estimates are all from this active region (also see Fig. 4). We note that this longitude was active for the preceding two solar rotations.

Also examined was the possibility that the value of A_{Ca} for an individual flare is correlated with other physical flare characteristics. In particular, the correlation between A_{Ca} and various flare and active region characteristics were studied:

1. The H α importance and the *GOES* soft X-ray classification;
2. Area of the sunspots in the related active region;
3. The duration, maximum, and total count rates recorded by the *SMM* Hard X-Ray Burst Spectrometer (Dennis et al. 1991);
4. Position of the flare in latitude and Carrington longitude;
5. Center-to-limb dependence;
6. Time and phase of the solar cycle;
7. Peak calcium temperature and emission measure;
8. Rise and decay characteristic times for calcium count rates, and calcium temperature and emission measure;
9. Ratio of decay to rise times (asymmetry) for the above mentioned parameters.

In no case was there a significant correlation detected. Figure 6 shows the values of A_{Ca} plotted against peak *GOES* X-ray flux for those flares where the *GOES* classification is known. The mean value of the entire sample (5.77×10^{-6}) is indicated as well as the photospheric value. Large flares have small scatter in values of A_{Ca} and are closer to the average for the entire sample.

The differences in the line-to-continuum measurements

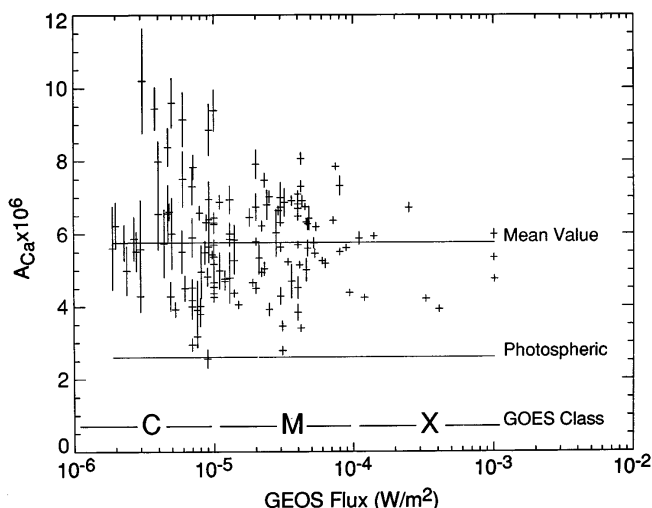


FIG. 6.—Values of A_{Ca} plotted against peak *GOES* X-ray flux for those flares for which the *GOES* classification is known. The upper horizontal line indicates the mean value of A_{Ca} of the entire sample of this analysis, and the lower horizontal line indicates the photospheric value.

have been interpreted in this work as evidence for a variation in the absolute calcium abundance on a flare-to-flare basis. Other possible causes for the variation in the observed ratio of F_w/F_c have been explored and are discussed below.

6.1. Instrumental

The *SMM*-BCS spectrometer was calibrated prior to launch and during the mission. Following the repair in 1984, the position gain in the calcium spectrometer began to change. The calibration results have been incorporated in the present analysis. Furthermore, the position gain does not affect the sensitivity of the detector (only its resolution), and so its effects are negligible for this study.

We have compared the *SMM*-BCS spectra with calcium spectra from the solar flare X-rays (SOLFLEX) spectrometer (Feldman, Doschek, & Kreplin 1980) on the P78-1 spacecraft. The line spectra measured with the two instruments are very similar. The continuum of the SOLFLEX spectrometer is contaminated by germanium fluorescence, however, so the two cannot be directly compared (Sterling et al. 1993).

6.2. Plasma Opacity

This present analysis is based on the intensity of the bright Ca XIX resonance line under the assumption that the thermal flare plasma is optically thin. If the plasma is not optically thin, then the intensity of the resonance line might be decreased relative to the continuum. The opacity at line center of a Doppler-broadened spectral line is given by (Sylwester et al. 1986b)

$$\tau_0 = N_e l \left(\frac{N_{Ca \text{ XIX}}}{N_{Ca}} \right) \left(\frac{N_{Ca}}{N_H} \right) \left(\frac{N_H}{N_e} \right) \left(\frac{\sqrt{\pi} e^2}{mc} \right) f \lambda \sqrt{\frac{\mu}{2RT}}, \quad (6)$$

where f is the oscillator strength for the w resonance line, m and e are the electron mass and charge, respectively, l is the length, R is the ideal gas constant, and μ is the atomic weight of calcium. For average flare conditions, if we assume $T = 15$ MK, $N_{Ca \text{ XIX}}/N_{Ca} = 0.86$, $A_{Ca} = 7 \times 10^{-6}$ and for the other quantities we take $N_H/N_e = 0.85$, $\lambda = 3.178$ Å, $f = 0.79$, and $\mu = 40.08$, then

$$\tau_0 = (2.4 \times 10^{-22}) N_e l. \quad (7)$$

A typical flaring loop has a length of 2×10^9 cm and a diameter that is 10 times smaller. Thus, if the line of sight is across the loop (perpendicular to the long axis of the loop), then for a density of $N_e = 5 \times 10^{11} \text{ cm}^{-3}$, we have $\tau_0 = 0.024$. The longest possible distance is one-half the loop length, which results in $\tau_0 = 0.12$. This is an extreme case, since flare loops normally have a temperature distribution with the hottest material at the loop top, and the peak in the Ca XIX emissivity function, $f_i(T)$ (see eq. [3]), occurs at around 35 MK. Observations of line w will preferentially be weighted toward the hot material near the loop top. Therefore, it can be concluded that opacity effects will be much less than 10%, and thus, this cannot be the reason for the observed variation in the line-to-continuum intensity ratio.

6.3. Nonequilibrium Ionization

The effects of transient ionization in solar flare plasma have been studied in a number of papers (Mewe & Schrijver 1980; Sylwester, Mewe, & Schrijver 1980a; Mewe et al. 1985). If the plasma is not in thermal equilibrium, it is more

difficult to interpret the observed X-ray spectrum. A detailed interpretation requires solving a coupled set of differential equations with time-dependent coefficients that vary with temperature and density. Under certain conditions, this can be simplified. For example, for the time during which a plasma is being heated, the characteristic time for ionization becomes important, whereas when the plasma is cooling, the recombination time should be considered. Mewe (1984) considered the ionization and recombination times as a function of temperature. These results are given in Table 4 for Ca XIX.

The temperature decay times for flares in this study were 5 minutes or more. For densities $10^{11} \text{ cm}^{-3} < N_e < 10^{12} \text{ cm}^{-3}$, which are typical for flare plasmas after the maximum (Wolfson et al. 1983; Sylwester et al. 1986a), τ_{rec} is of order 30 s or less, i.e., several times less than observed. Thus, the flare plasma can be considered in quasi-equilibrium during flare decay, and transient ionization effects can be considered unimportant for the purposes of this study. Spectra acquired during the flare rise phase were not included in this study.

6.4. Abundance Depletion of All Elements Except Calcium

The calculated continuum (eq. [4]) at 3.178 \AA depends weakly on the heavy elemental composition of the emitting plasma. The main effect from heavy elements comes from recombination of oxygen, neon, magnesium, and silicon. In order to test the effect of abundances on the solar thermal continuum, a computation was made assuming that all elements other than Ca and H had zero abundances. The effect on the computed F_w/F_c intensity ratio was less than 60%, and this can be ruled out as an explanation for the observed line-to-continuum variations. We can not rule out the possibility that the continuum has been affected by *increases* in non-Ca elemental abundances, such as helium, but this would not account for the observation of enhanced values of A_{Ca} relative to photospheric values.

6.5. Multithermal Plasma

Typical flare plasmas are multithermal, with temperature ranges extending to over 25 MK (see, e.g., Fludra & Schmelz 1995). The effect of multithermal plasma on the line-to-continuum analysis has been investigated by assuming the following form for the differential emission measure distribution to be $\varphi(T) = \text{const.}$ for $6 \text{ MK} < T < 25 \text{ MK}$. The Ca XIX line and continuum fluxes were calculated for this broad differential emission measure distribution. The resulting line fluxes were used to derive temperature and the calcium abundance of the simulated spectrum assuming an isothermal approximation. Checking this result shows that the isothermal approximation introduces an error in the abundance determination that is less

than 5%. Furthermore, Fludra et al. (1991) have calculated A_{Ca} for 12 flares from Table 1 using a method of multi-thermal analysis to obtain calcium abundances. Their results were the same, to within 3%, as those obtained from an isothermal analysis, which addresses the concern raised in Phillips & Feldman (1991).

7. SUMMARY

This paper presents final, detailed results of the study of variations in the line-to-continuum ratio in vicinity of the w line of Ca XIX ion using soft X-ray spectra from the BCS aboard the *SMM* satellite.

The analysis of thousands of spectra obtained during decay phases of more than 100 stronger flares revealed the presence of systematic differences in the line-to-continuum ratio between flares. This difference has been interpreted in terms of the varying Ca abundance hypothesis. Detailed considerations have ruled out other possible interpretations of the observed flare-to-flare variations of this ratio. The results obtained fully confirm the discovery of variations of coronal plasma composition from spectroscopic measurements (Sylwester et al. 1984). This discovery led to what is now one of the fastest growing areas of interest in solar physics—spectroscopic X-ray and EUV determinations of coronal plasma composition.

In this paper, absolute (relative to hydrogen) estimates of Ca abundance are given for flares observed during the period 1980–1987 by the BCS on the *SMM* spacecraft. The following conclusions may be drawn from this study:

1. Average flare calcium abundance (5.77×10^{-6}) is more than twice the photospheric value.
2. Flare-to-flare differences may amount to factor of ~ 3.5 ; the lowest flare abundance determined corresponds to the photospheric value (2.6×10^{-6}).
3. For most of flares, Ca abundance does not change during decay phase evolution.
4. Observed A_{Ca} variations do not correlate with any of the many commonly used flare and/or active region characteristics, except for the time trend seen for AR 2779.
5. For a particular active region, flare calcium abundances are similar; however, they may differ substantially from the abundances of flares for other active regions—the active region effect is clearly pronounced.

The observed pattern of flare abundance variations does not contradict the FIP-biased mechanism of coronal enrichment. As expected, the absolute abundance of Ca (a low-FIP element) in the corona is higher than in the photosphere. However, the time trend and active region effect of the present results impose substantial new limitations on the theoretical models of physical processes responsible for buildup of differences of the coronal plasma composition.

Recently, we (Bentley et al. 1998) have performed analyses of the flares observed with the BCS on the *Yohkoh* spacecraft. In this study, we considered more than 170 flares and have determined that for this group $A_{\text{Ca}} = 3.64 \times 10^{-6}$, which is closer to the photospheric value. A comparison of the *SMM* and *Yohkoh* data is in progress in order to evaluate the significance of these results.

The X-Ray Polychromator experiment was a collaborative program between Lockheed Palo Alto Research Laboratory, USA, the Mullard Space Science Laboratory,

TABLE 4

IONIZATION AND RECOMBINATION TIMES (IN s cm^{-3}) FOR THE CA XIX ION AT DIFFERENT TEMPERATURES

PARAMETER	T (MK)		
	8	15	25
$N_e \times \tau_{\text{ion}} \dots\dots$	8.6×10^{10}	2.7×10^{10}	1.4×10^{10}
$N_e \times \tau_{\text{rec}} \dots\dots$	2.0×10^{12}	2.8×10^{12}	3.6×10^{12}

UK, and the Rutherford Appleton Laboratory, UK. The authors thank Professor J. L. Culhane for useful discussions. J. S. acknowledges support for a part of this investigation from the British Council. J. R. L. acknowledges support from the Lockheed Martin Independent Research

Program. R. D. B., A. F., and M.-C. Z. acknowledge support from the UK Science and Engineering Research Council and the Particle Physics and Astrophysics Research Council.

REFERENCES

- Acton, L. W., et al. 1980, *Sol. Phys.*, 65, 53
 Allen, C. W. 1973, *Astrophysical Quantities* (3d ed.; London: Athlone)
 Antonucci, E., et al. 1982, *Sol. Phys.*, 78, 107
 Arnaud, J. 1984, *Proc. Fourth European Meeting on Solar Physics* (ESA SP-220) (Paris: ESA), 115
 Athay, R. G. 1986, *Physics of the Sun*, Vol. 2, ed. P. A. Sturrock (Dordrecht: Reidel), chap. 8
 Bely-Dubau, F., et al. 1982, *MNRAS*, 201, 1155
 Bentley, R. D., Sylwester, J., & Lemen, J. R. 1997, *Adv. Space Res.*, 20, 2275
 Dennis, B. R., et al., eds. 1991, *NASA Technical Memorandum 4332: The Complete Hard X-Ray Burst Spectrometer Event Listing 1980–1989* (Washington DC: NASA)
 Feldman, U. 1992, *Physica Scripta*, 46, 202
 Feldman, U., Doschek, G. A., & Kreplin, R. W. 1980, *ApJ*, 238, 365
 Fludra, A., Bentley, R. D., Culhane, J. L., Lemen, J. R., & Sylwester, J. 1991, *Adv. Space Res.*, 11(1), 155
 Fludra, A., Culhane, J. L., Bentley, R. D., Doschek, G. A., Hiei, E., Phillips, K. J. H., Sterling, A., & Watanabe, T. 1993, *Adv. Space Res.*, 13(9), 395
 Fludra, A., Lemen, J. R., Jakimiec, J., Bentley, R. D., & Sylwester, J. 1989, *ApJ*, 344, 991
 Fludra, A., & Schmelz, J. T. 1995, *ApJ*, 447, 936
 Geiss, J. 1982, *Space Sci. Rev.*, 33, 201
 Geiss, J., & Bochsler, P. 1986, in *The Sun and the Heliosphere in Three Dimensions*, ed. R. G. Marsden (Dordrecht: Reidel), 173
 Lemen, J. R., Phillips, K. J. H., Cowan, R. D., Hata, J., & Grant, I. P. 1984, *A&A*, 135, 313
 Lemen, J. R., Sylwester, J., & Bentley, R. D. 1986, *Adv. Space Res.*, 6(6), 245
 Lemen, J. R., Sylwester, J., Bentley, R. D., & Fludra, A. 1998, in preparation
 Mariska, J. T. 1980, *ApJ*, 235, 268
 Mason, H. E. 1975, *MNRAS*, 171, 119
 McGuire, R. E., von Rosevinge, T. T., & McDonald, F. B. 1985, *ApJ*, 301, 938
 Meyer, J. P. 1985a, *ApJS*, 57, 151
 ———. 1985b, *ApJS*, 57, 173
 ———. 1993, *Adv. Space Res.*, 13(9), 377
 Mewe, R., & Schrijver, J. 1980, *A&A*, 87, 261
 Mewe, R. 1984, *Physica Scripta*, T7, 5
 Mewe, R., Gronenschild, E. H. B. M., van den Oord, G. H. J., & Lemen, J. R. 1986, *A&AS*, 65, 511
 Mewe, R., Lemen, J. R., Peres, G., Schrijver, J., & Serio, S. 1985, *A&A*, 152, 229
 Parmar, A. N., Culhane, J. L., Rapley, C. G., Antonucci, E., Gabriel, A. H., & Loulergue, M. 1981, *MNRAS*, 197, 29P
 Parkinson, J. H. 1977, *A&A*, 57, 185
 Phillips, K. J. H., & Feldman, U. 1991, *ApJ*, 379, 401
 Pottash, S. R. 1964, *Space Sci. Rev.*, 3, 816
 Sterling, A., Doschek, G. A., & Feldman, U. 1993, *ApJ*, 404, 394
 Stone, E. C. 1989, in *AIP Conf. Proc. 183, Cosmic Abundances of Matter*, ed. C. J. Waddington (New York: AIP), 72
 Strong, K. T. 1988, *XRP Team Final Report: Contract NAS5-28713*
 Sylwester, B., Farnik, F., Sylwester, J., Jakimiec, J., & Valnicsek, B. 1986a, *Adv. Space Res.*, 6(6), 233
 Sylwester, B., et al. 1986b, *Sol. Phys.*, 103, 67
 Sylwester, J., Lemen, J. R., & Mewe, R. 1984, *Nature*, 310, 665
 Sylwester, J., Mewe, R., & Schrijver, J. 1980a, *A&AS*, 40, 335
 Sylwester, J., Schrijver, J., & Mewe, R. 1980b, *Sol. Phys.*, 67, 285
 Veck, N. J., & Parkinson, J. H. 1981, *MNRAS*, 197, 41
 Widing, K. G., & Feldman, U. 1989, *ApJ*, 344, 1046
 Wolfson, J., Doyle, J. G., Leibacher, J. W., & Phillips, K. J. H. 1983, *ApJ*, 269, 319